Dalton Transactions

PAPER

View Article Online
View Journal | View Issue

Cite this: *Dalton Trans.*, 2016, **45**, 667

Chirality at metal and helical ligand folding in optical isomers of chiral bis(naphthaldiminato)-nickel(II) complexes†

Mohammed Enamullah,*[a] Mohammad Abdul Quddus,[a] Mohammad Rezabul Hasan,[a] Gennaro Pescitelli,*[b] Roberto Berardozzi,[b] Gamall Makhloufi,[c] Vera Vasylyeva[c] and Christoph Janiak*[c]

Enantiopure bis[{(*R* or *S*)-*N*-1-(Ar)ethyl-2-oxo-1-naphthaldiminato-κ^2N,O}]nickel(II) complexes {Ar = C_6H_5 (**1*R*** or **1*S***), *p*-$OMeC_6H_4$ (**2*R*** or **2*S***), and *p*-BrC_6H_4 (**3*R*** or **3*S***)} are synthesized from the reactions between (*R* or *S*)-*N*-1-(Ar)ethyl-2-oxo-1-naphthaldimine and nickel(II) acetate. Circular-dichroism spectra and their density-functional theoretical simulation reveal the expected mirror image relationship between the enantiomeric pairs **1*R***/**1*S*** and **3*R***/**3*S*** in solution. CD spectra are dominated by the metal-centered *Λ*- or *Δ*-chirality of non-planar four-coordinated nickel, this latter being in turn dictated by the ligand chirality. Single crystal structure determination for **1*R*** and **1*S*** shows that there are two symmetry-independent molecules (**A** and **B**) in each asymmetric unit that give a $Z' = 2$ structure. Two asymmetric and chiral bidentate *N*^*O*-chelate Schiff base ligands coordinate to the nickel atom in a distorted square planar N_2O_2-coordination sphere. The conformational difference between the symmetry-independent molecules arises from the "up-or-down" folding of the naphthaldiminato ligand with respect to the coordination plane, which creates right- (*P*) or left-handed (*M*) helical conformations. Overall, the combination of ligand chirality, chirality at the metal and ligand folding gives rise to discrete metal helicates of preferred helicity in a selective way. Cyclic voltammograms (CV) show an oxidation wave at *ca.* 1.30 V for the $[Ni(L)_2]/[Ni(L)_2]^+$ couple, and a reduction wave at *ca.* −0.35 V for the $[Ni(L)_2]/[Ni(L)_2]^-$ couple in acetonitrile.

Received 8th October 2015,
Accepted 5th November 2015

DOI: 10.1039/c5dt03940a

www.rsc.org/dalton

Introduction

Chiral metal coordination complexes are the subject of continuous study due to their fascinating structures, and enormous potential applications such as in molecular recognition, non-linear optical materials, asymmetric catalysis, enantiomeric separation, and so on.[1,2] One of the possible ways of generating enantiopure chiral-at-metal complexes is the employment of chiral chelating ligands, which may then transfer their chirality to the metal centre(s) generating right- (*Δ*) or left-handed (*Λ*) helical structures in a stereocontrolled way.[3] The use of achiral chelating ligands usually results in a racemic mixture of left- and right-handed *Δ*/*Λ*-optical isomers.[4] Of special interest in the context of supramolecular chemistry are metal helicates, that is, metal complexes where one or more ligand "strands" wrap around one or more metal centres in a helical fashion.[5] In tetrahedral or distorted square-planar complexes the metal-centered chirality (*Λ vs.* *Δ*) can be induced with a C_2-symmetric structure by the use of an asymmetric ligand N^O to give $M(N^O)_2$ complexes (*cf.* Scheme 1).[6,7] An enantiomerically pure chelate ligand (*R* or *S*-N^O) often leads to the preferential formation of one diastereomer with absolute configuration of *Λ*(*R*,*R*) or *Δ*(*S*,*S*), while a racemic ligand gives both diastereomers {*e.g.* *Λ*(*R*,*R*) and *Δ*(*S*,*S*)}.[6–9]

We have recently paid attention to the phenomenon of helicity (*P vs.* *M*) and induced metal-centered chirality (*Λ vs.* *Δ*) in the complexes formed by the reaction of enantiopure amino acids and Schiff base ligands with Rh(I)[10,11] and Cu/Ni/Zn(II), respectively.[12–15] The most noteworthy finding in our studies is that the achiral *N*-phenylglycinate ligand coordinates to $[Rh(\eta^4\text{-cod})(acetate)]_2$ and gives a racemic chiral [Rh(η⁴-cod)(*N*-phenylglycinate)] complex with the nitrogen atom becoming a stereogenic center upon metal coordination.[10,11] The

[a]*Department of Chemistry, Jahangirnagar University, Dhaka-1342, Bangladesh. E-mail: enamullah@juniv.edu*
[b]*Department of Chemistry, University of Pisa, Via Moruzzi 13, 56124 Pisa, Italy. E-mail: gennaro.pescitelli@unipi.it*
[c]*Institut für Anorganische Chemie und Strukturchemie, Universität Düsseldorf, Universitätsstr. 1, D-40225 Düsseldorf, Germany. E-mail: janiak@uni-duesseldorf.de*
†Electronic supplementary information (ESI) available: ESI-MS data, ^{1}H-NMR spectra and data, cyclic voltammograms, analysis of supramolecular interactions, and CIF files reported in this paper. CCDC 1405162 and 1405163. For ESI and crystallographic data in CIF or other electronic format see DOI: 10.1039/c5dt03940a

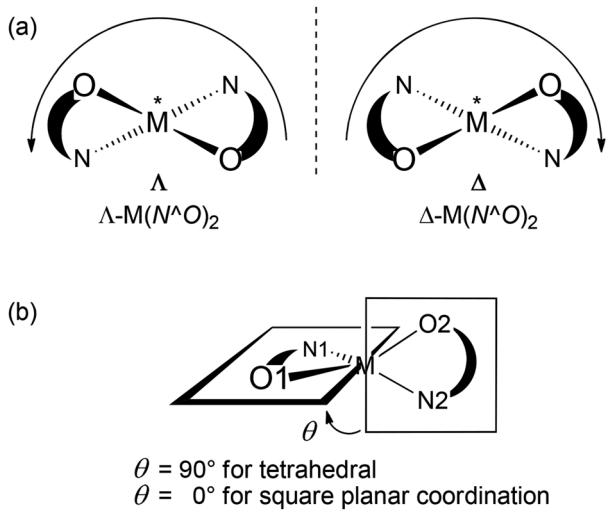

Scheme 1 Definition of (a) *Λ*/*Δ* chirality at the metal centre and (b) dihedral angle θ quantifying the deviation from tetrahedral or square planar geometry.

crystal structures reveal a case of two-fold spontaneous resolution of the racemic mixture into two homochiral helical enantiomers (helicates), namely the right-(*P*) and left-handed (*M*) helical chain structures with *S*- and *R*-*N*-phenylglycinate, respectively. Later, we have reported some examples of induced chirality at-metal-center with the preferential formation of the *Λ* or *Δ*-M configuration in distorted square planar M(*N*,*O*-chelate)$_2$ (*N*,*O*-chelate = enantiopure deprotonated Schiff base ligands; M = Cu, Ni, and Zn), which can be efficiently controlled by *R*- or *S*-chirality of the ligand.[12–14] Similarly, induced chirality at-metal-center in distorted square planar Cu/Zn(II) complexes with enantiopure or racemic amino alcohol-based Schiff base ligands was reported.[15] In particular, we have reported for the first time an example of induced chirality at-nickel-centre (*Δ vs. Λ*) in distorted octahedral, dinuclear μ-aqua-tetrakis{(*R* or *S*)-*N*-1-(Ar)ethyl-salicylaldiminato}-di-*Λ*- or *Δ*-nickel(II).[13]

The present paper reports the results of syntheses, spectroscopy, excited-state calculations and structural analyses of $Z' = 2$ helical structures of bis{(*R* or *S*)-*N*-1-(Ar)ethyl-2-oxo-1-naphthaldiminato-κ^2*N*,*O*}nickel(II) {Ar = C_6H_5, *p*-$OMeC_6H_4$, and *p*-BrC_6H_4}. The present complexes are structurally simpler than the related octahedral dinuclear analogs,[13] however, the specific folding of naphthaldiminato ligands around the metal centre gives rise to structurally intriguing discrete metal helicates.

Results and discussion

The enantiopure Schiff base ligands, (*R* or *S*)-*N*-1-(Ar)ethyl-2-oxo-1-naphthaldimine (*R* or *S*-HL), react with nickel(II)acetate to provide the bis[{(*R* or *S*)-*N*-1-(Ar)ethyl-2-oxo-1-naphthaldiminato-κ^2*N*,*O*}]nickel(II) complexes {Ar = C_6H_5 (Ni-*R*-L1; **1*R*** or Ni-*S*-L1; **1*S***), *p*-$OMeC_6H_4$ (Ni-*R*-L2; **2*R*** or Ni-*S*-L2; **2*S***), and *p*-BrC_6H_4 (Ni-*R*-L3; **3*R*** or Ni-*S*-L3; **3*S***)} (Scheme 2). Vibrational spectra show the main characteristic band at 1617–1604 cm^{-1} for the *ν*C=N stretching.[12–16,17] ESI-MS shows the parent ion peak at *m*/*z* 607 (**1*R*** or **1*S***) and 667 (**2*R*** or **2*S***) for $[M + H]^+$ species, while EI-MS shows this peak at *m*/*z* 764 (**3*R*** or **3*S***) for $[M]^+$. The spectra further show several ion peaks for $[M - HL]^+$, [HL or HL + H]$^+$ and different fragmented ligand species (Table S1†). ^{1}H NMR spectra (Fig. S1†) in $CDCl_3$ show a series of peaks expected for the C_2-symmetric four coordinated Ni(II)-complexes with a square planar geometry (see the Experimental section and the ESI†).[11,13,18–20] Notably, the imine (C*H*N) protons display large coordination shifts and appear as broad resonances above 11 ppm. The signal broadening, also seen to a smaller extent for other resonances, is probably due to solution paramagnetism. This

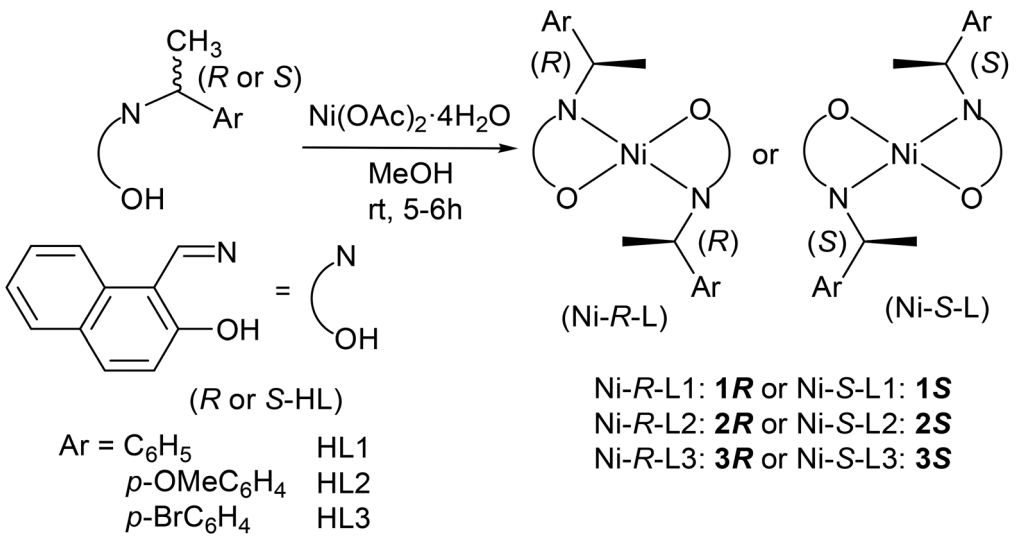

Scheme 2 Syntheses of the bis[{(*R* or *S*)-*N*-1-(Ar)ethyl-2-oxo-1-naphthaldiminato-κ^2*N*,*O*}]nickel(II).

is a well-known phenomenon for Ni(II) salicylideneaminato-complexes with bulky *N*-substituents and has been explained invoking a fast equilibrium between a dominant singlet species and a minor triplet species triggered by geometrical distortion (toward a tetrahedral geometry) and/or molecular association.[21]

Electronic spectra

UV-vis absorption and CD spectra of the complexes **1** and **3** measured in cyclohexane are shown in Fig. 1 and the spectral data are summarized in Table 1. All absorption spectra show consistent similarities over the whole measured range of 200–900 nm. In the visible region, there is a weak broad band around 600 nm followed by three bands of increasing intensity between 380–480, 330–380 and around 310 nm, respectively. They are followed by two more intense bands at 250–300 and below 250 nm. The band around 600 nm is due to the superposition of several metal-centred transitions typical of the Ni^{2+} core. The next bands in the UV region (<480 nm) involve a complex combination of several transitions, centred on both the metal and the ligands, as will be discussed below.

Electronic CD spectra of the enantiomeric couples **1*R*/1*S*** and **3*R*/3*S*** show the expected mirror-image relationship (Fig. 1 and Table 1) in cyclohexane. CD spectra display a larger variation between the two compounds as compared to the absorption spectra and also in comparison with the analogue Cu(II)-complexes.[12] In particular, in the visible range there is no distinctive feature immediately related to the ligand configuration for both **1** and **3**. The only consistent signals are in the UV region, and they are (for *R* configuration, Fig. 1 and Table 1) the weak positive band between 400 and 450 nm, the stronger negative band at 300–330 nm, and the strong positive band below 220 nm.

We also measured solid-state CD spectra of crystalline samples of compound **1**, but found them to be not fully reproducible. Moreover, in the case of the analogous Cu complexes,[12] we demonstrated that solid-state CD spectra are dominated by inter-crystalline couplings and do not reflect in a simple way the molecular conformation.

Simulating the solution CD spectra of Ni complexes **1–3** by means of CD calculations is a laborious task because of the inherent complexity of the system[22] and the uncertainty of the solution structures. Therefore, the work described in the

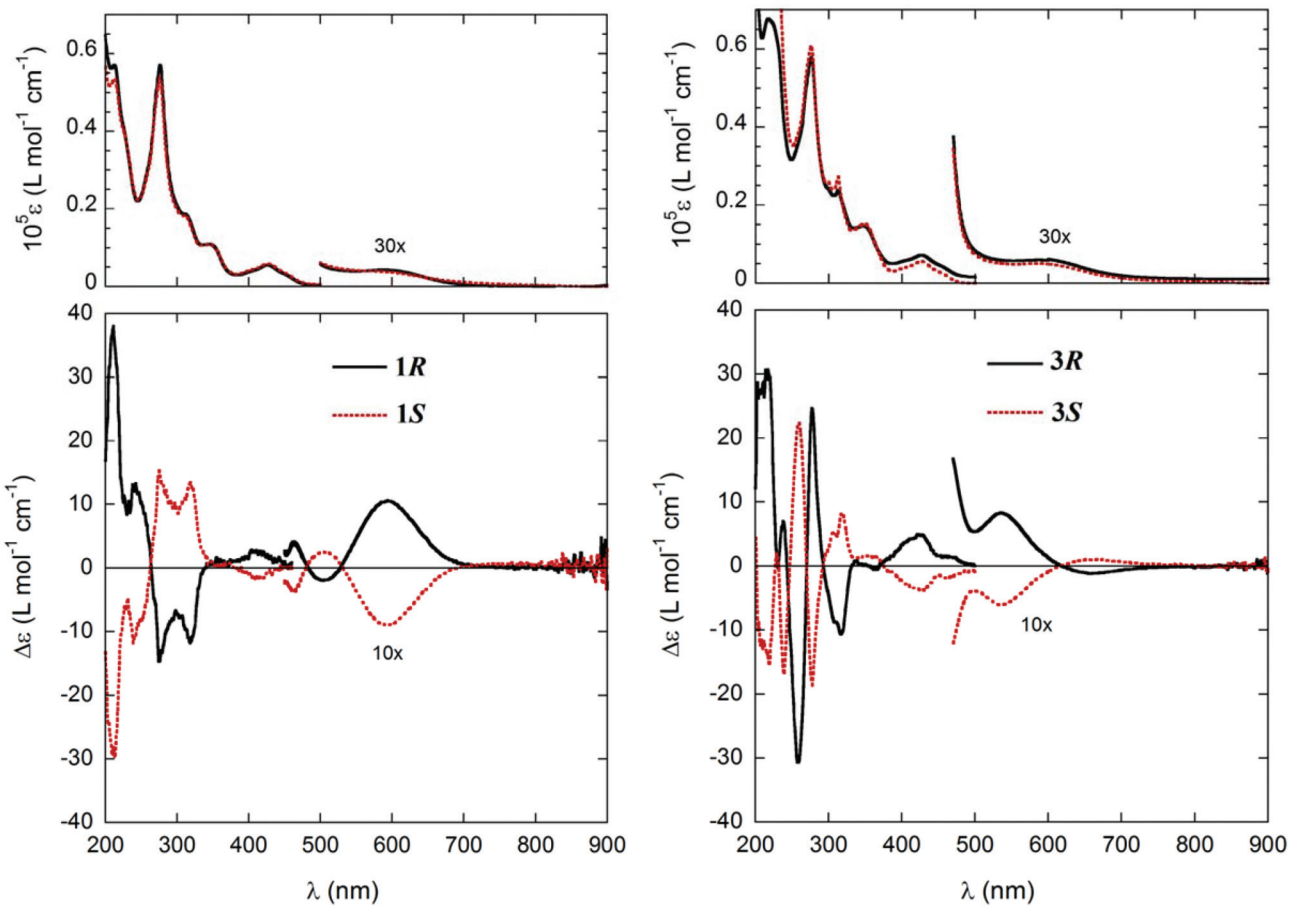

Fig. 1 UV-vis. and CD spectra of **1*R*** (0.76 mM), **1*S*** (0.79 mM) (left), and **3*R*** (1.95 mM), **3*S*** (1.96 mM) (right) in cyclohexane; cell path-length: 0.1 mm, 200–500 nm; 5 mm, 425–600 nm; 10 mm, 400–900 nm.

Table 1 UV-vis and CD spectral data of **1*R*/1*S*** and **3*R*/3*S*** in cyclohexane; cell path-length: 0.1 mm (200–500 nm); 5–10 mm (400–900 nm) at 20 °C

Compounds	Spectra	Bands[a]
1*R*/1*S*	UV-vis	588 (vw), 427 (m), 345 (s), 312 (s), 276 (vs), and 212 (vs) nm
3*R*/3*S*	UV-vis	595 (vw), 425 (m), 348 (s), 312 (s), 277 (vs), and 220 (vs) nm
1*R*/1*S*	CD	590 (+/–, w), 505 (–/+, vw), 460 (+/–, vw), 410 (+/–, w), 317 (–/+, s), 276 (–/+, s), 240 (+/–, s), and 210 (+/–, vs) nm
3*R*/3*S*	CD	660 (–/+, vw), 534 (+/–, w), 425 (+/–, s), 313 (–/+, s), 278 (+/–, vs), 256 (–/+, vs), 237 (+/–, m), and 213 (+/–, vs) nm

[a] vw = very weak, w = weak, m = medium, s = strong, vs = very strong.

following section aimed mainly at establishing the relationship between the observed CD spectra and the chirality at both carbon centres and the metal ion (if any), in analogy with our previous work on Cu analogues.[12] Although the solid-state structures of **1*R*** and **1*S*** show only a faint chirality at the Ni atoms (see below), the situation in solution may in principle be different. The chirality at the metal centre is defined as shown in Scheme 1a, and the distortion from an ideal tetrahedral or square-planar geometry can be quantified by the dihedral angle θ between the two planes formed by the donor atoms with the metal atom, that is, N1–M–O1 and N2–M–O2 (Scheme 1b). Starting from the X-ray structure of **1*R***, we investigated the solution conformation of this complex by means of a conformational search using molecular mechanics and DFT geometry optimizations at the B3LYP/6-31G(d) level (see the Computational section). The resulting most stable structure showed a small but detectable angle $\theta = -10.8°$ corresponding to ***Λ*-Ni-1*R*** chirality, and resembled strongly molecule **A** found in the X-ray discussed below (inset in Fig. 2A); other conformations had much higher energies and were neglected. Starting from the same complex, the chirality at the metal centre was inverted and the same conformational search/geometry optimization procedure was applied. The set of structures with ***Δ*-Ni-1*R*** chirality thus obtained showed two low-energy conformations, one (more stable) with $\theta = 15.0°$ and the second (less stable by 0.16 kcal mol^{-1}) with $\theta = 9.0°$ (see the ESI†). Interestingly, the lowest-energy ***Λ*-Ni-1*R*** structure was more stable by about 1.7 kcal mol^{-1} than the ***Δ*-Ni-1*R*** one. Thus, a small but non-negligible diastereomeric preference in favour of the ***Λ*-Ni-1*R*** isomer is predicted, similarly to what was observed for the Cu analogues.[12] To confirm this finding, CD calculations were run with the TDDFT method[23] at the B3LYP/TZVP level on the above described structures (Fig. 2). The most striking observation from Fig. 2 is that the CD spectra calculated for ***Λ*-Ni-1*R*** and ***Δ*-Ni-1*R*** are almost the mirror image of each other on a wide wavelength range. This demonstrates that the CD spectrum in solution is dominated by the metal chirality, this latter being in turn dictated by the ligand chirality. Second, the CD spectrum calculated for ***Λ*-Ni-1*R*** is in reasonable agreement with the experimental one for compound **1*R***. As mentioned above, a perfect agreement cannot be expected because of the system complexity and the very large number of transitions contributing to the spectrum (80 excited states were included in the TDDFT calculations, which are

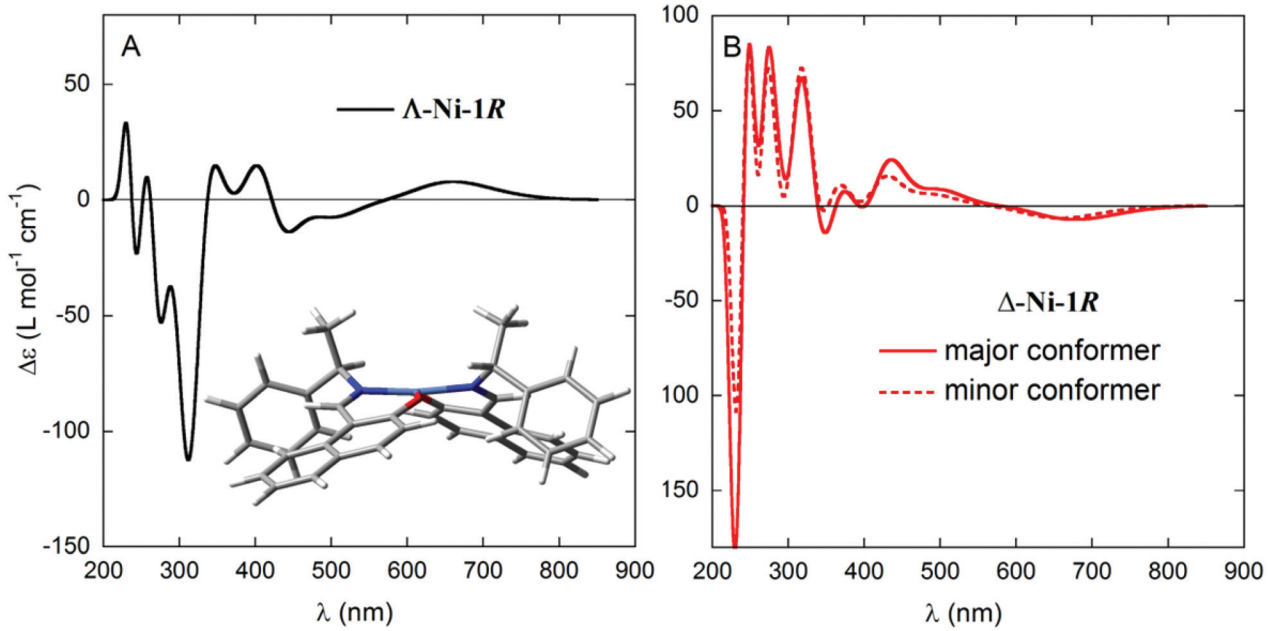

Fig. 2 CD spectra, calculated at the B3LYP/TZVP//B3LYP/6-31G(d) level, for the two diastereomers ***Λ*-Ni-1*R*** (left, conformation shown in the inset) and ***Δ*-Ni-1*R*** (right, two conformations shown in Fig. S3†). Gaussian band shape with exponential bandwidth $\sigma = 0.2$ eV.

Table 2 Main transitions calculated for the *Λ*-Ni-1*R* complex with B3LYP/TZVP//B3LYP/6-31G(d), contribution to the first observed CD bands, and simplified assignment

Exc. state	Calculated transition wavelength (nm)	Observed CD band (maximum wavelength, nm, and sign)	Assignment[a]
1	660	590 (+)	M–M
3	514	505 (−)	M–M, L–M, CT
4	498		CT, M–M
5	428		M–M
6	414	460 (+)	M–M
7 + 8	359	410 (+)	M–M
9	344		M–M, L–M
10	336		M–M, L–M
13	322	317 (−)	M–M
15	309		M–L

[a] Legend: M–M, metal d–d; L–M, ligand-to-metal; M–L, metal-to-ligand; CT, charge transfer; in order of importance.

intrinsically poorly accurate for high-lying transitions).[24] The comparison between experimental and calculated CD spectra allows us to confirm that the complex obtained from ligand *R*-L1 assumes a predominant ***Λ*-Ni-1*R*** configuration in solution, and the same is inferred for the remaining ligands.

We have already stressed[12,13] that for d-metal complexes containing chromophoric ligands rich in transitions, such as compounds **1–3**, a straightforward assignment of electronic spectra in terms of purely metal- or ligand-centred transitions is not possible. On the basis of orbital and population analyses of compound **1*R*** at the B3LYP/TZVP level, the simplified assignment shown in Table 2 was reached, concerning only the transitions that contributed the most to the CD spectrum above 300 nm. It is important to notice, however, that every transition is derived from many single excitations, and there is no clear separation between metal-centred and ligand-centred transitions, because several metal-centred transitions occur deeply in the UV region of the spectrum.

Solid state structural studies

Single crystal X-ray structure determination for Ni-*R*-L1 (**1*R***) and Ni-*S*-L1 (**1*S***) shows that there are two symmetry-independent molecules in each asymmetric unit, that is, molecule **A** with Ni1 and molecule **B** with the Ni2 centre in each unit. In each structure, two bidentate *N^O*-chelate Schiff base ligands coordinate to the nickel atom with a square planar N_2O_2-coordination sphere around the metal atom (Fig. 3). The two nitrogen atoms (and subsequently the two oxygen atoms) are *trans* positioned. The Ni–O/N bond lengths and O–Ni–N bond angles are listed in Table 3 and are as expected for analogous Ni(II)-Schiff base complexes.[8,13] Despite the presence of aromatic rings in the complexes Ni-*R*-L1 (**1*R***) and Ni-*S*-L1 (**1*S***), there are no detectable π–π interactions[25] but intermolecular C–H···π contacts[26] are evident in the packings; a detailed analysis is reported in the ESI.†

Two symmetry-independent Ni-Schiff base molecules or, more correctly, two identical chemical formula units were found here in the structural asymmetric unit[27] to give a $Z' = 2$ structure. The definition of Z' is that it refers to the number of formula units in the unit cell (here 4) divided by the number of independent general positions (here 2).[28] Different reasons can lead to such $Z' > 1$ structures:[29] a structure stuck *en-route* to a more stable form,[28] that is, a crystal "on the way",[27,30–32] or strong and special supramolecular (*e.g.* hydrogen bonding) interactions between the two (or more) symmetry-independent units.[33–38] A high Z' is also obtained when the molecule has different equi-energetic conformations, with these conformations co-existing in the crystal.[39,40] The chance for $Z' > 1$ is higher in non-centrosymmetric space groups with (enantiopure) chiral molecules which have difficulties in packing efficiently in the absence of centrosymmetry.[41]

Different from our previous studies on four-coordinated Cu(II) with asymmetric (N^O) and chiral Schiff base ligands[12,42] the distortion from square-planar geometry, as assessed by the dihedral angle *θ* (*cf.* Scheme 1b) at the Ni atoms in **1*R*** and **1*S*** is very small. The dihedral angle *θ* is only 10° for molecules **A** and less than 2° for molecules **B**. The experimental angle of about 10° agrees well with the angle of 10.8° obtained from DFT geometry optimizations at the B3LYP/6-31G(d) level for *Λ*-Ni-*R*-L1 (**1*R***) (see above). This difference in the dihedral angle *θ* could explain the formation of the two independent molecules **A** and **B**. The two molecules **A** and **B**, after relaxation of the hydrogen atoms at the B3LYP/6-31G(d) level, have different DFT energies, molecule **A** being more stable by 1.8 kcal mol^{-1}. This is similar to the difference found between fully optimized ***Λ*-** and ***Δ*-Ni-1*R*** structures described above.

Yet, the conformational difference between the two symmetry independent molecules **A** and **B** is better explained with the help of Scheme 3. Each Ni-naphthaldiminato half does not assume a planar arrangement. Instead, each six-membered $NiNOC_3$ chelate ring is folded "up-or-down" hinging on the N···O vector to assume an envelope conformation.[43] In each molecule **A** and **B**, the folding of the two chelate rings occurs on the same side of the NiN_2O_2 plane. The folding angles *ϕ*, that is, the angles defined by the NiN_2O_2 plane and each of the naphthaldiminato planes (Scheme 3), are listed in Table 4. The folding in molecule **A** with Ni1 is more pronounced with very similar folding angles of $\phi \sim 21°$ than in molecule **B** with Ni2 which has smaller and two different folding angles of 5° and 16°. An overlay of both molecules in each structure illustrates the different folding directions (Fig. 4). The folding angles measured for DFT-optimized structures are also listed in Table 4, and they agree well with the values measured for molecule **A** in the crystals.

The combination of the folding in the $NiNOC_3$ ring, the intrinsic curvature in the naphthaldiminato ligand, and the concurrence of these two phenomena for the two ligands, creates an overall complex conformation around the nickel atom which has a helical appearance. The helicity can be differentiated into right-handed (*P*) or left-handed (*M*) as shown in Scheme 3. With their different "up-or-down" folding

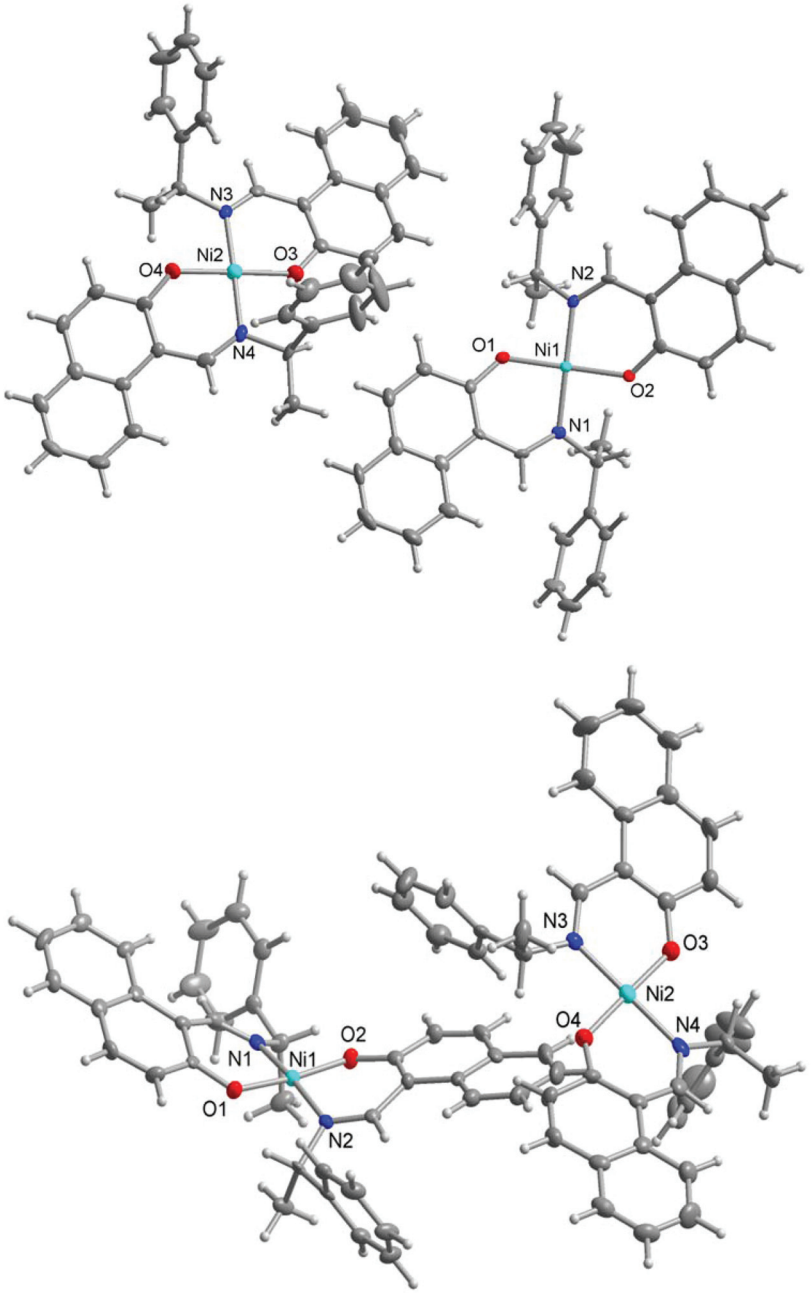

Fig. 3 Structures of the two symmetry-independent molecules of the enantiomeric couple Ni-*R*-L1 (**1*R***) (above) and Ni-*S*-L1 (**1*S***) (below). Thermal ellipsoids are at the 70% level. See Table 3 for bond lengths and angles.

the two symmetry-independent molecules **A** and **B** found in the crystal assume a different helicity. For example, in Ni-*R*-L1 (**1*R***) the molecule with Ni1 is *M*-helical, the molecule with Ni2 is *P*-helical, and *vice versa* in Ni-*S*-L1 (**1*S***) (Scheme 3). This *P*- or *M*-conformational helicity is in addition to the *Λ*- or *Δ*-metal-centred chirality. It is noteworthy that the left-handed *M*-conformation with a large folding angle ϕ of about 21° goes together with a more distinct dihedral angle θ of 10° for the clearly *Λ*-chiral molecule **A** in **1*R*** (and conversely the right-handed *P* with the clearly *Δ*-chiral molecule **A** in **1*S***). However, the right-handed *P*-conformation with the smaller and uneven folding angles ϕ of 5° and 16° combines with the barely recognizable *Λ*-chiral molecule **B** in **1*R*** which has only a very small dihedral angle $\theta < 2°$, that is, essentially square planar (and it is the other way round for *M* which combines with the barely recognizable *Δ*-chiral molecule **B** in **1*S***) (see Scheme 3). The two angles θ and ϕ, describing together the deviation from an ideal square planar metal geometry for all-planar naphthaldiminato ligands, appear to be correlated with each other. The essentially square-planar Ni configuration in the **B** molecules

Table 3 Selected bond lengths (Å) and angles (°) in the compounds[a]

Ni-*R*-L1 (**1*R***)				Ni-*S*-L1 (**1*S***)			
1*R* (A)				**1*S* (A)**			
Ni(1)–O(1)	1.848(2)	O(1)–Ni(1)–O(2)	172.73(10)	Ni(1)–O(1)	1.840(3)	O(1)–Ni(1)–O(2)	172.94(8)
Ni(1)–O(2)	1.850(2)	O(1)–Ni(1)–N(1)	92.16(11)	Ni(1)–O(2)	1.835(2)	O(1)–Ni(1)–N(1)	91.94(10)
Ni(1)–N(1)	1.908(3)	O(2)–Ni(1)–N(1)	88.35(11)	Ni(1)–N(1)	1.909(3)	O(2)–Ni(1)–N(1)	88.44(10)
Ni(1)–N(2)	1.914(3)	O(1)–Ni(1)–N(2)	88.39(11)	Ni(1)–N(2)	1.901(3)	O(1)–Ni(1)–N(2)	88.43(10)
		O(2)–Ni(1)–N(2)	92.01(11)			O(2)–Ni(1)–N(2)	92.08(10)
		N(1)–Ni(1)–N(2)	172.85(11)			N(1)–Ni(1)–N(2)	172.72(12)
1*R* (B)				**1*S* (B)**			
Ni(2)–O(3)	1.818(2)	O(3)–Ni(2)–O(4)	179.39(12)	Ni(2)–O(3)	1.817(3)	O(3)–Ni(2)–O(4)	179.33(10)
Ni(2)–O(4)	1.828(2)	O(3)–Ni(2)–N(3)	92.08(11)	Ni(2)–O(4)	1.823(3)	O(3)–Ni(2)–N(3)	92.01(10)
Ni(2)–N(3)	1.946(3)	O(4)–Ni(2)–N(3)	88.52(11)	Ni(2)–N(3)	1.935(3)	O(4)–Ni(2)–N(3)	88.6(1)
Ni(2)–N(4)	1.963(3)	O(3)–Ni(2)–N(4)	88.74(11)	Ni(2)–N(4)	1.953(3)	O(3)–Ni(2)–N(4)	88.8(1)
		O(4)–Ni(2)–N(4)	90.66(11)			O(4)–Ni(2)–N(4)	90.6(1)
		N(3)–Ni(2)–N(4)	178.02(12)			N(3)–Ni(2)–N(4)	178.11(11)

[a] **A** and **B** refer to the two symmetry independent molecules in each of the structure.

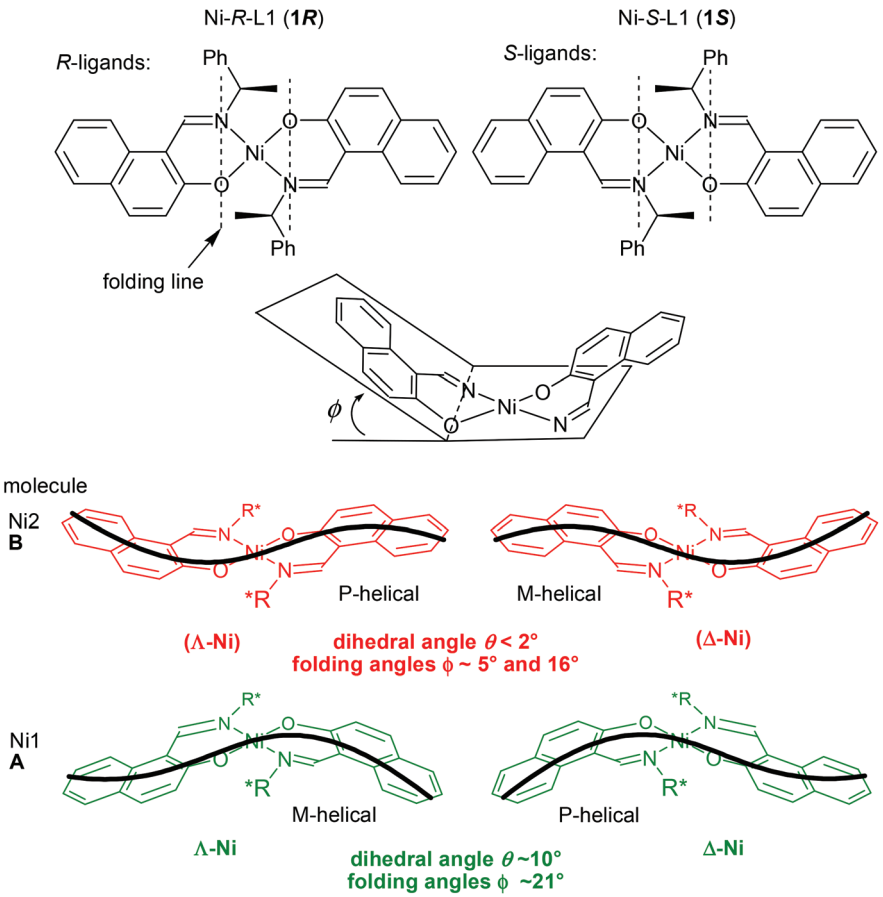

Scheme 3 Schematic illustration of the non-planar, skewed bis(naphthaldiminato) N_2O_2 ligand arrangement around the nearly square-planar coordinated Ni atom in **1*R*** (left) and **1*S*** (right) and definition of the folding angle ϕ. The thick black line depicts the *P*- or *M*-helical arrangement from the envelope conformation in the $NiNOC_3$ chelate ring together with the curvature in the naphthaldiminato ligand. The round brackets indicate a faint chirality at Ni.

Table 4 Dihedral and folding angles for the two symmetry independent molecules (**A**, **B**) in Ni-*R*-L1 (**1*R***) and Ni-*S*-L1 (**1*S***), respectively

Complexes (molecule)	Chirality at Ni[a]	θ (°)[b] exp.	θ (°)[b] calc.[c]	ϕ (°)[d] exp.		ϕ (°)[d] calc.[c]
1*R* (**A**, Ni1)	Λ	10.0(1)	10.8 Λ	20.6(1)	21.8(10)	25.3 Λ
1*R* (**B**, Ni2)	(Λ)	1.80(9)		5.1(1)	16.1(1)	
1*S* (**A**, Ni1)	Δ	9.98(9)	10.8 Δ	20.8(1)	21.8(1)	25.3 Δ
1*S* (**B**, Ni2)	(Δ)	1.73(9)		5.28(8)	16.4(1)	

[a] The round brackets indicate a faint chirality at Ni. [b] Dihedral angle θ between the two planes is formed by the donor atoms with the metal atom (*cf.* Scheme 1), that is, N1–Ni–O1 and N2–Ni–O2 (molecule **A**) and respective numbering in molecule **B**. [c] By DFT geometry optimizations at the B3LYP/6-31G(d) level; the calculated chirality at Ni is also given. [d] Folding angle is defined as the angle between O–Ni–N and O–C–C–C–N (*cf.* Scheme 3) with all these atoms forming the six-membered $NiNOC_3$ chelate ring. Each chelate ring has a folding angle, hence, there are two independent folding angles in a molecule.

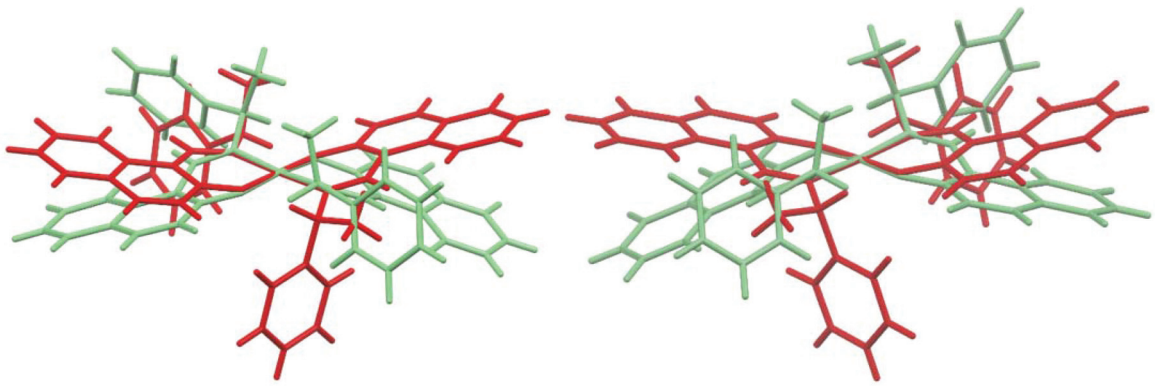

Fig. 4 Overlay of the two symmetry independent molecules in Ni-*R*-L1 (**1*R***) (left) and Ni-*S*-L1 (**1*S***) (right). The Ni1 molecule **A** is shown in green, the Ni2 molecule **B** in red. The five atoms NiN_2O_2 are pairwise specified to orient the overlay which is managed with the "Structure overlay" option in Mercury 3.5.1 (copyright CCDC 2001–2014, http://www.ccdc.cam.ac.uk/mercury/).

in **1*R*** and **1*S*** may be seen as an effort of the *P*- (in **1*R***) and *M*-configurations (in **1*S***) to invert the Ni configuration. Evidently *P* prefers to have Δ at Ni and *M* prefers having Λ. This is confirmed by DFT results and by CD spectroscopy. Our DFT structures (see the Electronic Spectra section and Table 4) show a strong prevalence for the Δ(Ni)/*P* (or Λ(Ni)/*M*) combination. The DFT lowest energy structure has large dihedral θ and folding ϕ angles, with absolute values very similar to those

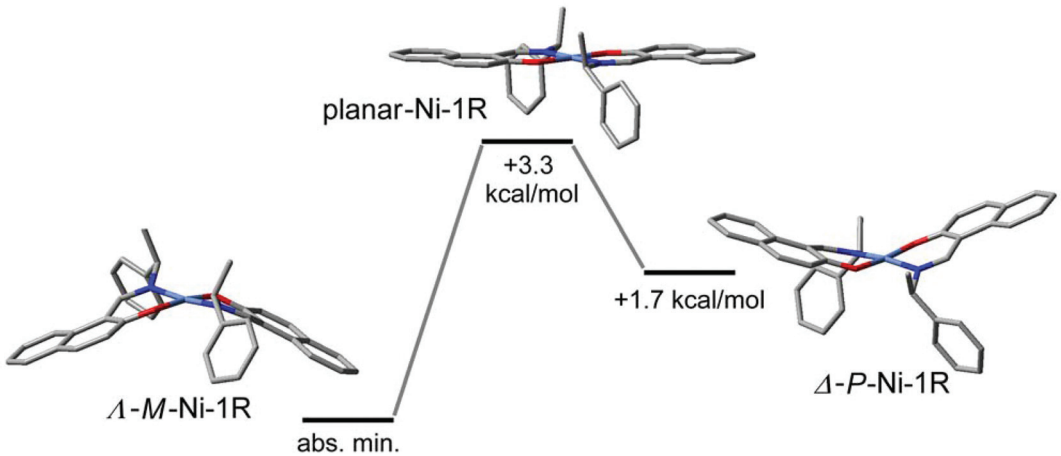

Fig. 5 Sketch of the interconversion process between Λ-**Ni-1*R*** (*M*-helical) and Δ-**Ni-1*R*** (*P*-helical) structures in solution, passing through a planar intermediate (devoid of metal chirality and helicity). Geometry optimizations and energies are calculated at the B3LYP/6-31G(d) level; the middle structure is optimized by constraining the Ni(bis-naphthaldiminato) moiety into a planar conformation. Hydrogen atoms are omitted for clarity.

measured for molecule **A**. In turn, solution CD spectra and CD calculations give clear evidence that the *Λ*- (in **1*R***) and *Δ*-configurations (in **1*S***) are mostly retained (although they could partly invert upon the conformational rearrangement).[14,41] Further studies are necessary to detect and quantify any inversion phenomenon occurring in solution. Possibly, the *P*- and *M*-conformational helicities may invert dynamically in solution akin to a bird's flap with its wings, as sketched in Fig. 5. The structure with an all-planar Ni(bis-naphthaldiminato) moiety (in the middle of Fig. 5), though not necessarily coinciding with the real transition state, offers an estimate of the conversion barrier (around 3.5 kcal mol^{-1}) between the *P*- and *M*-conformational isomers of compound **1*R***, allowing for a very fast process. Very likely, the unfavorable *P* (in **1*R***) and *M*-configurations (in **1*S***) in the crystals invert upon dissolution. It should be noted that the chelate-ring folding, when idealized, maintains the C_2-symmetry of the molecule.

Thermally induced structural phase transformation

Thermally induced structural phase transformation has been reported for transition metal–chiral *N*,*O*-chelate complexes, accompanying a change from a distorted square planar/tetrahedral geometry in the solid state to a regular square planar/tetrahedral geometry in the isotropic liquid phase.[8a–d,12,13,15,21,44–46] Differential Scanning Calorimetry (DSC) has successfully been used to study the phenomenon. Thus DSC heating curves of the present compounds show an exothermic peak at *ca.* 190 °C for **1*S***, **3*R***, **3*S*** and at 141 °C for **2*R*** (Fig. 6 and Table 5), while cooling curves show no corresponding peak in the reverse direction. The results demonstrate a thermally induced irreversible phase transformation as reported for the analogous Ni(II)-*N*,*O*-chelate complexes.[8c,d,13]

Cyclic voltammetry

Cyclic voltammograms (CV) of the free Schiff base (*S*-HL1) and compounds **1*S*** and **3*R*** were recorded in the range of −0.50 to 1.50 V *versus* Ag/AgCl in acetonitrile using different switching potentials at varying scan rates (Fig. 7 and the ESI†). The free

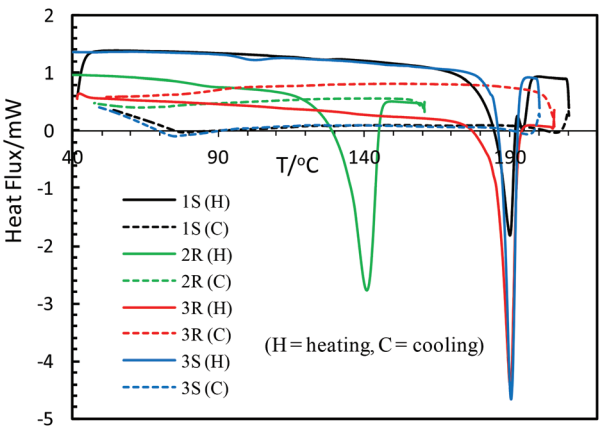

Fig. 6 DSC analysis curves of heating and cooling for the compounds.

Table 5 Thermally induced structural phase transformation data for the compounds

Compounds (physical appearance)	Peaks (*T*/°C)	ΔH (kJ mol^{-1})
1*S* (dark brown block shaped crystals)	190.1[a]	−33.01
2*R* (greenish microcrystals)	140.8	−28.03
3*R* (greenish microcrystals)	190.2	−36.34
3*S* (greenish microcrystals)	190.7	−42.62

[a] The reported value is 183 °C for the analogous [(*R*)-*N*-1-(phenyl)ethyl-X-salicylaldiminato]Ni(II).[8d]

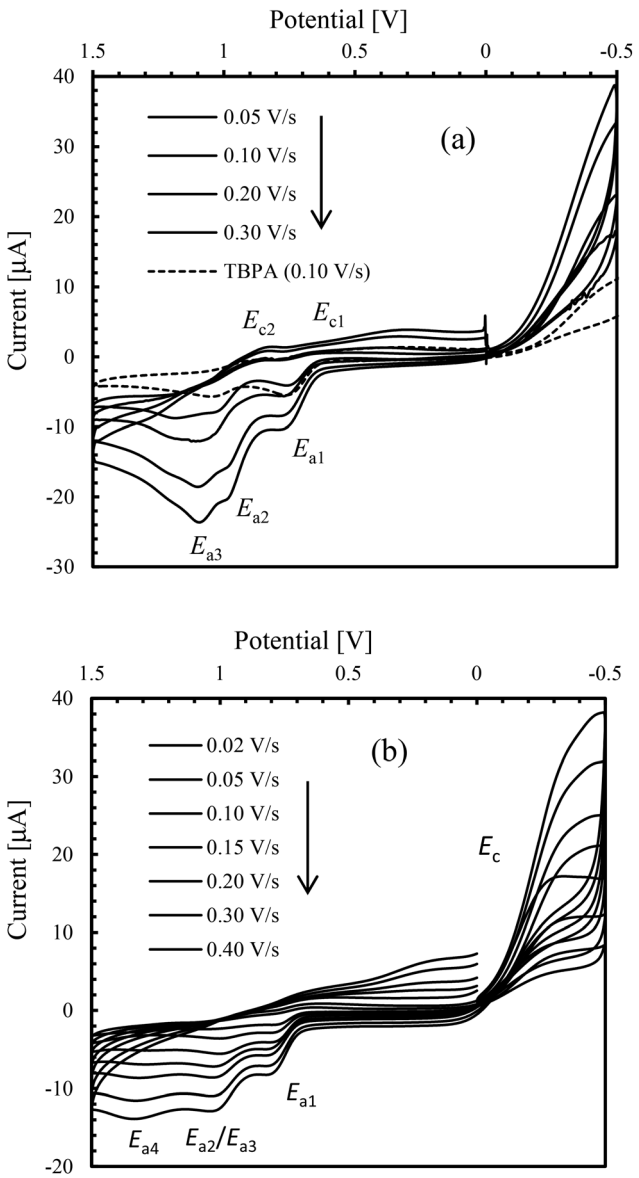

Fig. 7 Cyclic voltammograms of (a) *S*-HL1 (1.5 mmol L^{-1}) and (b) **1*S*** (1.0 mmol L^{-1}); TBAP (0.1 mol L^{-1}) at varying scan rates in acetonitrile at 25 °C.

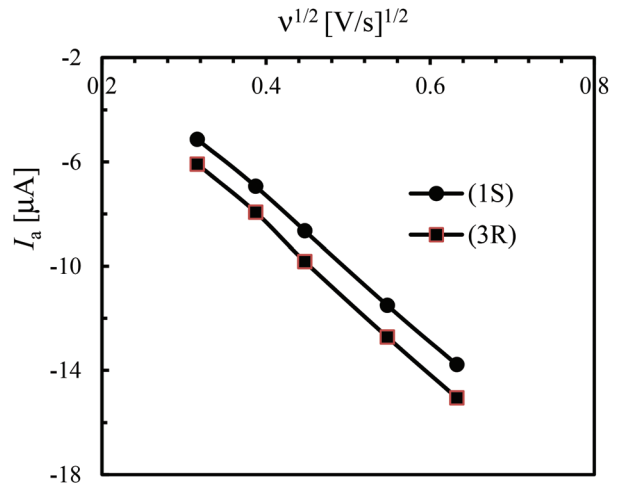

Fig. 8 Change of anodic current (I_a) at *ca.* 1.30 V *vs.* square root of the scan rate, ($\nu^{1/2}$).

Schiff base solution shows three anodic waves at *ca.* E_{a1} = 0.73, E_{a2} = 1.00 and E_{a3} = 1.20 V (Fig. 7a). Among them the former two waves are also seen for the electrolyte (TBAP) solution (Fig. 7a, dashed line), which shows the corresponding reduction waves at *ca.* E_{c1} = 0.70 and E_{c2} = 0.90 V. Hence, the latter wave (E_{a3}) is due to the oxidation of the free Schiff base ligand. Voltammograms of **1*S***, **2*R*** and **3*R*** (Fig. 7b and the ESI†) are identical and show an additional anodic wave at *ca.* 1.30 V (E_{a4}), which becomes more significant at higher scan rates, and is associated with the oxidation wave for the $[Ni(L)_2]/[Ni(L)_2]^+$ couple.[47,48] However, the corresponding cathodic wave is not detected even at higher scan rates, because of the instability of the cationic species ($[Ni(L)_2]^+$) which undergoes a rapid irreversible reaction to produce an electrode-inactive species.[47a] The voltammograms in the cathodic region (*i.e.*, 0 to −0.50 V) show a reduction wave at *ca.* −0.35 V (E_c) for the $[Ni(L)_2]/[Ni(L)_2]^-$ couple (Fig. 7b and the ESI†), which overlaps with the decomposition peak of the electrolyte (TBAP) at higher scan rates.[48a] In fact, a corresponding poor oxidation wave is seen in the reverse scan, which undergoes rapid chemical transformation due to the instability of the $[Ni(L)_2]^-$ species. Analysis of voltammograms at varying scan rates (0.02 to 0.40 V s^{-1}) demonstrates a linear relationship between the anodic peak current (I_a) at *ca.* 1.30 V and the square root of the scan rate ($\nu^{1/2}$, Fig. 8), indicating a diffusion-controlled electrochemical process.

Conclusions

We have reported the synthesis, characterization, X-ray structure, and computational study of a series of chiral bis-(naphthaldiminato)Ni(II) complexes **1–3** with a distorted square planar geometry around the metal ion. These complexes show a remarkable stereochemistry because the ligand configuration is selectively and concurrently transferred to the metal chirality and to the conformational helicity of the ligands. Thus, a ligand with *R* configuration favors the formation of a complex with *Λ* chirality at the Ni and *M* ligand helicity. The stereochemical behavior of our series of complexes may be of interest in different fields based on the multiplication and amplification of chirality. First, the chiral folding of the naphthaldiminato moieties imparts the complexes with a discrete helicity which may be the starting point to obtain supramolecular helicates in a very selective and efficient way.[5] Second, the complexes are possibly expected to induce high twisting powers when used as dopants for cholesteric liquid crystals.[49]

Experimental section

IR-spectra were recorded on a Nicolet iS10 spectrometer as KBr discs at ambient temperature. UV-Vis. spectra were obtained with a Shimadzu UV 1800 spectrophotometer in cyclohexane at 25 °C. Elemental analyses were performed on a Vario EL instrument from Elementar Analysensysteme. An Epsilon™ Instruments (BASi) electrochemical analyzer was used for cyclic voltammetry (CV) experiments containing tetra-*N*-butylammonium-hexafluorophosphate (TBAP) as the supporting electrolyte in acetonitrile at 25 °C. The three-electrode measurement was carried out with a platinum disc working electrode, a platinum wire auxiliary electrode and an Ag/AgCl reference electrode. The solution containing the compounds and TBAP was deoxygenated for 10 minutes by passing nitrogen gas prior to running the experiments. CD spectra were obtained with a JASCO spectropolarimeter (J715) in cyclohexane on 2–2.5 mM samples. For each solution sample, three distinct spectra were recorded using cells with different path-lengths (0.1 mm, 5 mm and 10 mm) to cover the whole spectral range from 190–200 to 900 nm by keeping the absorbance below 1.5 AU. ^{1}H-NMR spectra were run on a Bruker Avance DPX 400 spectrometer (operating at 400 MHz, ^{1}H) in $CDCl_3$ (δ 7.25 ppm) at 20 °C. EI-MS: Thermo-Finnigan TSQ 700. Isotopic distribution patterns for $^{58/60}$Ni (in **1*R*/*S*** and **2*R*/*S***) or combined $^{63/65}$Ni + $^{79/81}$Br (in **3*R*/*S***) containing ions are clearly visible in the mass spectra.

General procedure to synthesise the complexes

Two equivalents of enantiopure (*R* or *S*)-*N*-1-(C_6H_5)ethyl-2-oxo-1-naphthaldimine (*R* or *S*-HL1) (341 mg, 1.24 mmol) dissolved in 5 mL methanol were added into a 5 mL hot methanolic solution of $Ni(O_2CCH_3)_2{\cdot}4H_2O$ (154 mg, 0.62 mmol) and the solution was stirred for 6–8 h at room temperature. The color changes from light green to greenish brown in clear solution. The volume of the solvent was reduced to *ca.* 50%, and this clear solution was left standing for crystallization *via* slow solvent evaporation of the solvent at room temperature. Dark brown block shaped crystals of Ni-*R*-L1 (**1*R***) or Ni-*S*-L1 (**1*S***), suitable for X-ray measurement, were obtained within 5–6 d. The crystals were separated, washed with methanol (2 × 2 mL), and dried in air for 3–4 d. The same procedure was followed for the syntheses of Ni-*R*-L2 (**2*R***) or Ni-*S*-L2 (**2*S***) using

the Schiff bases of (*R* or *S*)-*N*-1-(*p*-OMeC$_6$H$_4$)ethyl-2-oxo-1-naphthaldimine (*R* or *S*-HL2), and greenish microcrystals were obtained after 5–6 d, that were not suitable for X-ray measurement. For the syntheses of Ni-*R*-L3 (**3*R***) or Ni-*S*-L3 (**3*S***) using (*R* or *S*)-*N*-1-(*p*-BrC$_6$H$_4$)ethyl-2-oxo-1-naphthaldimine (*R* or *S*-HL3), a green precipitate was formed within 30 min of stirring the solution. Stirring was continued for 6–8 h, and this solution was left standing for 8–10 h until complete precipitation. The solution was filtered off, and the precipitate was washed with methanol (2 × 2 mL). Green microcrystals of Ni-*R*-L3 (**3*R***) or Ni-*S*-L3 (**3*S***) were obtained after drying the sample in air for 3–4 d.

Bis{(*R*)-*N*-1-(C$_6$H$_5$)ethyl-2-oxo-1-naphthaldiminato-κ^2*N*,*O*}-nickel(II) (Ni-*R*-L1; 1*R*). Dark brown block shaped crystals. Yield 275 mg (73%). IR (KBr, cm^{-1}): ν = 3057, 3027, 2971w (H–C), 1617, 1605vs (C=N), and 1541s (C=C). ^{1}H NMR (400 MHz, $CDCl_3$): δ = 1.97 (d, J = 6.5 Hz, 6H, C*H*$_3$), 6.64 (d, J = 9.2 Hz, 2H), 6.78 (t, J = 7.4 Hz, 2H), 7.05 (d, J = 8.4 Hz, 2H), 7.34 (d, J = 8.4 Hz, 4H), 7.42 (t, J = 7.4 Hz, 4H), 7.60 (m, 6H), 7.74 (d, J = 8.8 Hz, 2H), and 11.05 (s, 2H, C*H*N). ESI-MS: 607 (30) [M + H]$^+$, 331 (58) [M − HL1]$^+$, 228 (100) [C$_{10}$H$_6$(CHNH)(O)Ni] and 105 (33) [CH(C$_6$H$_5$)(CH$_3$)]$^+$. $C_{38}H_{32}N_2O_2Ni$ (607.40): calcd C 75.14, H 5.31, N 4.61; found C 75.35, H 5.04, N 4.36.

Bis{(*S*)-*N*-1-(C$_6$H$_5$)ethyl-2-oxo-1-naphthaldiminato-κ^2*N*,*O*}-nickel(II) (Ni-*S*-L1; 1*S*). Dark brown block shaped crystals. Yield 260 mg (67%). IR (KBr, cm^{-1}): ν = 3055, 3032, 2970w (H–C), 1616, 1605vs (C=N), and 1540s (C=C). ^{1}H NMR (400 MHz, $CDCl_3$): δ = 1.97 (d, J = 6.5 Hz, 6H, C*H*$_3$), 6.62 (d, J = 9.2 Hz, 2H), 6.76 (t, J = 7.4 Hz, 2H), 7.05 (d, J = 8.4 Hz, 2H), 7.32 (d, J = 8.4 Hz, 4H), 7.41 (t, J = 7.4 Hz, 4H), 7.59 (m, 6H), 7.72 (d, J = 8.8 Hz, 2H), and 11.02 (br, 2H). ESI-MS: 607 (20) [M + H]$^+$, 331 (45) [M − HL1]$^+$, 228 (100) [C$_{10}$H$_6$(CHNH)(O)Ni] and 105 (25) [CH(C$_6$H$_5$)(CH$_3$)]$^+$. $C_{38}H_{32}N_2O_2Ni\cdot H_2O$ (625.41): calcd C 72.98, H 5.48, N 4.48; found C 71.46, H 4.86, N 4.34.

Bis{(*R*)-*N*-1-(*p*-OMeC$_6$H$_4$)ethyl-2-oxo-1-naphthaldiminato-κ^2*N*,*O*}nickel(II) (Ni-*R*-L2; 2*R*). Greenish microcrystals. Yield 300 mg (72%). IR (KBr, cm^{-1}): ν = 3052, 3043w (H–Ar), 1624, 1605vs (C=N), and 1541s (C=C). ^{1}H NMR (400 MHz, $CDCl_3$): δ = 2.01 (d, J = 6.5 Hz, 6H, C*H*$_3$), 3.83 (s, 6H, OC*H*$_3$), 6.56 (d, J = 7.2 Hz, 2H), 6.96 (m, 6H), 7.09 (d, J = 8.4 Hz, 2H), 7.36 (d, J = 8.4 Hz, 2H), 7.56 (d, J = 7.4 Hz, 4H), 7.61 (d, J = 8.4 Hz, 2H), 7.88 (d, J = 8.8 Hz, 2H), and 12.81 (br, 2H). ESI-MS: 667 (15) [M + H]$^+$, 306 (10) [HL2 + H]$^+$, 135 (100) [CH(CH$_3$)(C$_6$H$_4$OCH$_3$)]$^+$ and 105 (15) [CH(C$_6$H$_5$)(CH$_3$)]$^+$. $C_{40}H_{36}N_2O_4Ni$ (667.45): calcd C 71.98, H 5.44, N 4.20; found C 71.32, H 5.29, N 4.12.

Bis{(*S*)-*N*-1-(*p*-OMeC$_6$H$_4$)ethyl-2-oxo-1-naphthaldiminato-κ^2*N*,*O*}nickel(II) (Ni-*S*-L2; 2*S*). Greenish microcrystals. Yield 280 mg (68%). IR (KBr, cm^{-1}): ν = 3050, 3025w (H–Ar), 1642, 1611vs (C=N), and 1541s (C=C). ESI-MS: 667 (5) [M + H]$^+$, 306 (10) [HL2 + H]$^+$, 135 (100) [CH(CH$_3$)(C$_6$H$_4$OCH$_3$)]$^+$ and 105 (20) [CH(C$_6$H$_5$)(CH$_3$)]$^+$. $C_{40}H_{36}N_2O_4Ni$ (667.45): calcd C 71.98, H 5.44, N 4.20; found C 71.43, H 5.30, N 4.09.

Bis{(*R*)-*N*-1-(*p*-BrC$_6$H$_4$)ethyl-2-oxo-1-naphthaldiminato-κ^2*N*,*O*}-nickel(II) (Ni-*R*-L3; 3*R*). Greenish microcrystals. Yield 360 mg (72%). IR (KBr, cm^{-1}): ν = 3051, 3027, 2973w (H–C), 1616, 1607vs (C=N), and 1541s (C=C). ^{1}H NMR (400 MHz, $CDCl_3$): δ = 1.94 (d, J = 6.0 Hz, 6H, C*H*$_3$), 6.63 (d, J = 8.8 Hz, 2H), 6.88 (d, J = 7.2 Hz, 2H), 7.12 (t, J = 6.8 Hz, 2H), 7.37 (d, J = 7.4 Hz, 4H), 7.55 (d, J = 8.4 Hz, 6H), 7.67 (d, J = 7.0 Hz, 2H), 7.82 (d, J = 8.4 Hz, 2H), and 11.27 (br, 2H). $C_{38}H_{30}N_2O_2Br_2Ni\cdot 2H_2O$ (801.24): calcd C 56.96, H 4.28, N 3.50; found C 56.24, H 3.86, N 3.40.

Bis{(*S*)-*N*-1-(*p*-BrC$_6$H$_4$)ethyl-2-oxo-1-naphthaldiminato-κ^2*N*,*O*}-nickel(II) (Ni-*S*-L3; 3*S*). Greenish microcrystals. Yield 350 mg (70%). IR (KBr, cm^{-1}): ν = 3057, 3030, 2972w (H–C), 1616, 1605vs (C=N), and 1541s (C=C). EI-MS (70 eV): m/z (%) = 764 (10) [M]$^+$, 411 (100) [M − HL3]$^+$, 353 (30) [HL3]$^+$, 229 (20) [C$_{10}$H$_6$(O)(CHNH)Ni + H]$^+$, 183 (35) [C$_6$H$_4$(Br)(CHCH$_3$)]$^+$, 170 (60) [C$_{10}$H$_6$(O)(CHNH)]$^+$, and 104 (60) [CH$_3$CHC$_6$H$_5$–H]$^+$ (isotopic distribution pattern resulting from the combination of $^{58/60}$Ni+$^{79/81}$Br containing ions is clearly visible following the peaks at 764, 411, 229 while for $^{79/81}$Br containing ions at 353, and 183). $C_{38}H_{30}N_2O_2Br_2Ni\cdot 2H_2O$ (801.24): calcd C 56.96, H 4.28, N 3.50; found C 56.04, H 3.66, N 3.42).

X-ray crystallography

Single-crystals of enantiomeric pairs Ni-*R*-L1 (**1*R***) and Ni-*S*-L1 (**1*S***) were carefully selected under a polarizing microscope and mounted on a loop. *Data collection*: Bruker APEX II CCD diffractometer with multi-layer mirror-monochromated Mo-Kα radiation (λ = 0.71073 Å) at 203(2) K; ω-scans (see Table 6). Data collection and cell refinement with APEX2,[50] data reduction with SAINT (Bruker).[51] *Structure analysis and refinement*: the structures were solved by direct methods (SHELXS-97),[52] refinement was done by full-matrix least squares on F^2 using the SHELXL-97 program suite,[52] empirical (multi-scan) absorption correction with SADABS (Bruker).[53] All non-hydrogen positions were refined with anisotropic temperature factors. Hydrogen atoms for aromatic CH, aliphatic or olefinic CH, CH$_2$ and OH groups were positioned geometrically (C–H = 0.94 Å for aromatic CH, C–H = 0.94 Å for olefinic CH, 0.99 for aliphatic CH and 0.97 Å for CH$_3$), and refined using a riding model (AFIX 43 for aromatic CH, AFIX 13 for aliphatic CH, AFIX 137 for CH$_3$), with U_{iso}(H) = 1.2U_{eq}(CH, CH$_2$) and U_{iso}(H) = 1.5U_{eq}(CH$_3$). Details of the X-ray structure determination and refinements are provided in Table 6. Graphics were drawn with DIAMOND (Version 3.2).[54] Computations on the supramolecular interactions were carried out with PLATON for Windows.[55] The structural data for this paper have been deposited with the Cambridge Crystallographic Data Center (CCDC numbers 1405162 and 1405163).

Computational section

Conformational searches and geometry optimizations were run with Spartan'14 (Wave function, Inc. Irvine, CA). Excited-state CD calculations were run with Gaussian09.[56] Initial structures were generated starting from the available X-ray structure of the **Λ-Ni-1*R*** complex. An initial structure with an opposite configuration at the metal, **Δ-Ni-1*R***, was obtained by mirror inversion of the whole complex, followed by a second inversion of the carbon chirality centers only. Conformational searches were run with molecular mechanics, using the Molecular Merck Force Field (MMFF). The geometry around the metal

Table 6 Crystal data and structure refinement for the compounds

	Ni-*R*-L1 (**1*R***)	Ni-*S*-L1 (**1*S***)
Empirical formula	$C_{38}H_{32}N_2O_2Ni$	$C_{38}H_{32}N_2O_2Ni$
M/g mol^{-1}	607.37	607.37
Crystal size/mm^3	0.072 × 0.072 × 0.067	0.56 × 0.36 × 0.11
Temperature/K	95	100
θ range/°(completeness)	1.97–27.50 (99.8%)	1.66–25.23 (99.1%)
h; k; l range	−8,12; −15, 19; ±26	±11; ±18; ±24
Crystal system	Monoclinic	Monoclinic
Space group	$P2_1$ (no. 4)	$P2_1$ (no. 4)
a/Å	9.5282(16)	9.5328(9)
b/Å	15.355(3)	15.2970(16)
c/Å	20.655(4)	20.560(2)
β/°	90.146(7)	90.192(6)
V/Å^3	3021.93(10)	2998.1(5)
Z/D_{calc}(g cm^{-3})	4/1.335	4/1.346
μ (Mo Kα)/mm^{-1}	0.679	0.685
F(000)	1272	1272
Max./min. transmission	0.956/0.953	0.700/0.928
Reflections collected	28 227	25 081
Independent reflect. (R_{int})	12217 (0.0617)	10664 (0.0573)
Data/restraints/parameters	12217/13/779	10 664/1/779
Max./min. $\Delta\rho^a$/e Å^{-3}	0.688/−0.948	0.394/−0.661
R_1/wR_2 [$I > 2\sigma(I)$]^b	0.0494/0.0944	0.0384/0.0922
R_1/wR_2 (all data)^b	0.0678/0.1016	0.0438/0.0945
Goodness-of-fit on $F^{2\,c}$	0.991	1.006
Flack parameter^d	0.008(10)	0.040(8)

^{a} Largest difference peak and hole. ^{b} $R_1 = [\sum(||F_o| - |F_c||)/\sum|F_o|]$; w$R_2 = [\sum[w(F_o^2 - F_c^2)^2]/\sum[w(F_o^2)^2]]^{1/2}$. ^{c} Goodness-of-fit $= [\sum[w(F_o^2 - F_c^2)^2]/(n-p)]^{1/2}$. ^{d} Absolute structure parameter.[59]

was kept fixed by constraining the O–Ni and N–Ni bond lengths and the O–Ni–O and N–Ni–N bond angles at their respective X-ray values. All the remaining rotatable bonds were included in the conformational search (*i.e.*, varied systematically) and optimized with MMFF. All structures thus obtained were fully re-optimized with DFT using the B3LYP functional with the 6-31G(d) basis set on all atoms.[57] Excited state calculations were run with the TDDFT method. A preliminary set of calculations was run to test the performance of various DFT functionals and basis sets, including a limited number of excited states (roots). The following functionals were tested: B3LYP, CAM-B3LYP, M06, PBE1PBE, wB97X-D and the two basis sets SVP and TZVP.[56] Final calculations including 80 roots were run with the B3LYP/TZVP combination. The spectra were generated using the program SpecDis[58] by applying a Gaussian band shape with a 0.2 eV exponential half-width. Rotational strengths calculated with a dipole-length gauge were employed, the differences between dipole-velocity values being negligible for most transitions.

Acknowledgements

We acknowledge the financial support from the Ministry of Science and Technology (MOST) under the project 2012/13, Dhaka, Bangladesh. We acknowledge the "Wazed Miah Science Research Centre" at Jahangirnagar University, Dhaka, Bangladesh for obtaining CV and elemental data. G.P. thanks Prof. Fabio Marchetti and Dr Francesco Zinna for useful discussions.

Notes and references

1 (*a*) J. D. Watson and F. H. C. Crick, *Nature*, 1953, **171**, 737; (*b*) T. Nakano and Y. Okamoto, *Chem. Rev.*, 2001, **101**, 4013; (*c*) L. Pauling, R. B. Corey and H. R. Branson, *Proc. Natl. Acad. Sci. U. S. A.*, 1951, **37**, 205; (*d*) N. Chen, M.-X. Li, P. Yang, X. He, M. Shao and S.-R. Zhu, *Cryst. Growth Des.*, 2013, **13**, 2650; (*e*) Z. Chen, S. Qin, D. Liu, Y. Shen and F. Liang, *Cryst. Growth Des.*, 2013, **13**, 3389; (*f*) W.-W. He, J. Yang, Y. Yang, Y.-Y. Liu and J.-F. Ma, *Dalton Trans.*, 2012, **41**, 9737; (*g*) K. Kano and H. Hasegawa, *J. Am. Chem. Soc.*, 2001, **123**, 10616; (*h*) W.-G. Lu, J.-Z. Gu, L. Jiang, M.-Y. Tan and T.-B. Lu, *Cryst. Growth Des.*, 2008, **8**, 192; (*i*) L.-L. Wen, D.-B. Dang, C.-Y. Duan, Y.-Z. Li, Z.-F. Tian and Q.-J. Meng, *Inorg. Chem.*, 2005, **44**, 7161; (*j*) D.-R. Xiao, E.-B. Wang, H.-Y. An, Y.-G. Li, Z.-M. Su and C.-Y. Sun, *Chem. – Eur. J.*, 2006, **12**, 6528; (*k*) Y. Cui, O. R. Evans, H. L. Ngo, P. S. White and W. Lin, *Angew. Chem., Int. Ed.*, 2002, **41**, 1159.

2 (*a*) H. Hou, X. Meng, Y. Song, Y. Fan, Y. Zhu, H. Lu, C. Du and W. Shao, *Inorg. Chem.*, 2002, **41**, 4068; (*b*) A. C. Kathalikkattil, K. K. Bisht, N. Aliaga-Alcalde and E. Suresh, *Cryst. Growth Des.*, 2011, **11**, 1631; (*c*) S. Kitagawa, R. Kitaura and S.-I. Noro, *Angew. Chem., Int. Ed.*, 2004, **43**, 2334; (*d*) S. J. Lee, A. Hu and W. Lin, *J. Am. Chem. Soc.*, 2002, **124**, 12948; (*e*) W. Lin, Z. Wang and L. Ma, *J. Am. Chem. Soc.*, 1999, **121**, 11249; (*f*) X. Meng, Y. Song, H. Hou, Y. Fan, G. Li and Y. Zhu, *Inorg. Chem.*, 2003, **42**, 1306; (*g*) J. S. Seo, D. Whang, H. Lee, S. I. Jun, J. Oh, Y. J. Jeon and K. Kim, *Nature*, 2000, **404**, 982; (*h*) P. J. Deuss, R. den Heeten, W. Laan and P. C. J. Kamer, *Chem. – Eur. J.*, 2011, **17**, 4680; (*i*) J. Crassous, *Chem. Soc. Rev.*, 2009, **38**, 830.

3 (*a*) E. V. Anokhina and A. J. Jacobson, *J. Am. Chem. Soc.*, 2004, **126**, 3044; (*b*) S. P. Anthony and T. P. Radhakrishnan, *Chem. Commun.*, 2004, 1058; (*c*) J. Heo, Y.-M. Jeon and C. A. Mirkin, *J. Am. Chem. Soc.*, 2007, **129**, 7712; (*d*) L. Jiang, X.-L. Feng, C.-Y. Su, X.-M. Chen and T.-B. Lu, *Inorg. Chem.*, 2007, **46**, 2637; L. Jiang, T.-B. Lu and X.-L. Feng, *Inorg. Chem.*, 2005, **44**, 7056; (*e*) L. Ohrstrom, K. Larsson, S. Borg and S. T. Norberg, *Chem. – Eur. J.*, 2001, **7**, 4805; (*f*) A. Roth, D. Koth, M. Gottschaldt and W. Plass, *Cryst. Growth Des.*, 2006, **6**, 2655.

4 (*a*) C. S. Isfort, T. Kreickmann, T. Pape, R. Froehlich and F. E. Hahn, *Chem. – Eur. J.*, 2007, **13**, 2344; (*b*) H.-J. Kim, E. Lee, H.-S. Park and M. Lee, *J. Am. Chem. Soc.*, 2007, **129**, 10994; (*c*) R. Wang, Y. Zhou, Y. Sun, D. Yuan, L. Han, B. Lou, B. Wu and M. Hong, *Cryst. Growth Des.*, 2005, **5**, 25; (*d*) S.-T. Wu, Y.-R. Wu, Q.-Q. Kang, H. Zhang, L.-S. Long, Z. Zheng, R.-B. Huang and L.-S. Zheng, *Angew. Chem., Int.*

Ed., 2007, **46**, 8475; (*e*) Y. Zhang, J. Li, J. Chen, Q. Su, W. Deng, M. Nishiura, T. Imamoto, X. Wu and Q. Wang, *Inorg. Chem.*, 2000, **39**, 2330.

5 (*a*) J.-M. Lehn, A. Rigault, J. Siegel, J. Harrowfield, B. Chevrier and D. Moras, *Proc. Natl. Acad. Sci. U. S. A.*, 1987, **84**, 2565; (*b*) M. Albrecht, *Chem. Soc. Rev.*, 2001, **101**, 3457; (*c*) C. Biswas, M. G. B. Drew, M. Estrader and A. Ghosh, *Dalton Trans.*, 2009, 5015; (*d*) F. Lin, H.-Y. Peng, J.-X. Chen, D. T. W. Chik, Z. Cai, K. M. C. Wong, V. W. W. Yam and H. N. C. Wong, *J. Am. Chem. Soc.*, 2010, **132**, 16383.

6 (*a*) U. Knof and A. von Zelewsky, *Angew. Chem., Int. Ed.*, 1999, **38**, 302–322; (*b*) A. von Zelewsky and O. Mamula, *J. Chem. Soc., Dalton Trans.*, 2000, 219–231; (*c*) P. J. Steel, *J. Org. Chem.*, 1991, **408**, 395–402; (*d*) P. Hayoz and A. von Zelewsky, *Tetrahedron Lett.*, 1992, **33:36**, 5165–5168; (*e*) R. Vadavi, E. D. Conrad, D. I. Arbuckle, T. S. Cameron, E. Essoun and M. A. S. Aquino, *Inorg. Chem.*, 2011, **50**, 11862–11864; (*f*) B. R. Groves, D. I. Arbuckle, E. Essoun, T. L. Lundrigan, R. Wang and M. A. S. Aquino, *Inorg. Chem.*, 2013, **52**, 11563–11572; (*g*) L. J. Boudreau, T. L. Clarke, A. H. Murray, K. N. Robertson, T. S. Cameron and M. A. S. Aquino, *Inorg. Chim. Acta*, 2013, **394**, 152–158; (*h*) E. C. Constable, G. Zhang, C. E. Housecroft, M. Neuburger and J. A. Zampese, *Chem. Commun.*, 2010, 3077–3079; (*i*) E. C. Constable, C. E. Housecroft, T. Kulke, C. Lazzarini, E. R. Schofield and Y. Zimmermann, *J. Chem. Soc., Dalton Trans.*, 2001, 2864–2871.

7 (*a*) K. Warnmark, J. A. Thomas, O. Heyke and J.-M. Lehn, *Chem. Commun.*, 1996, 701–702; (*b*) F. M. MacDonnell and S. Bodige, *Inorg. Chem.*, 1996, **35**, 5758–5759; (*c*) S. Bodige, A. S. Torres, D. J. Maloney, D. Tale, G. R. Kinsel, A. K. Walker and F. M. MacDonnell, *J. Am. Chem. Soc.*, 1997, **119**, 10364–10369; (*d*) K. Wärnmark, O. Heyke, J. A. Thomas and J.-M. Lehn, *Chem. Commun.*, 1996, 2603–2604; (*e*) T. J. Rutherford, M. G. Quagliotto and F. R. Keene, *Inorg. Chem.*, 1995, **34**, 3857–3858; (*f*) D. Tzalis and Y. Tor, *J. Am. Chem. Soc.*, 1997, **119**, 852–853.

8 (*a*) T. Akitsu and Y. Einaga, *Polyhedron*, 2005, **24**, 2933–2943; (*b*) G.-P. Li, Q.-C. Yang, Y.-Q. Tang, Y.-D. Guan and Z.-H. Shang, *Acta Chim. Sin.*, 1987, **45**, 421–425; (*c*) T. Akitsu, *Polyhedron*, 2007, **26**, 2527–2535; (*d*) T. Akitsu and Y. Einaga, *Polyhedron*, 2005, **24**, 1869–1877; (*e*) T. Akitsu and Y. Einaga, *Acta Crystallogr., Sect. C: Cryst. Struct. Commun.*, 2004, **60**, m640–m642; (*f*) H. Sakiyama, H. Okawa, N. Matsumoto and S. Kida, *J. Chem. Soc., Dalton Trans.*, 1990, 2935–2939; (*g*) C. Evans and D. Luneau, *J. Chem. Soc., Dalton Trans.*, 2002, 83–86; (*h*) H. Sakiyama, H. Okawa, N. Matsumoto and S. Kida, *Bull. Chem. Soc. Jpn.*, 1991, **64**, 2644–2647.

9 (*a*) F. Wang, H. Zhang, L. Li, H.-Q. Hao, X.-Y. Wang and J.-G. Chen, *Tetrahedron: Asymmetry*, 2006, **17**, 2059–2063; (*b*) H. S. Chow, E. C. Constable, R. Frantz, C. E. Housecroft, J. Lacour, M. Neuburger, D. Rappoport and S. Schaffner, *New J. Chem.*, 2009, **33**, 376–385; (*c*) G. Brewer, C. Brewer, R. J. Butcher, G. T. Robichaux and C. Viragh, *Inorg. Chim. Acta*, 2014, **410**, 171–177; (*d*) E. C. Constable, C. E. Housecroft, V. Jullien, M. Neuburger, I. Poleschak, S. Reymann, S. Saxer and S. Schaffner, *Polyhedron*, 2007, **26**, 5519–5526; (*e*) E. C. Constable, *Chem. Soc. Rev.*, 2013, **42**, 1637–1651.

10 M. Enamullah, A. Sharmin, M. Hasegawa, T. Hoshi, A.-C. Chamayou and C. Janiak, *Eur. J. Inorg. Chem.*, 2006, 2146–2154.

11 C. Janiak, A.-C. Chamayou, A. K. M. Royhan Uddin, M. Uddin, K. S. Hagen and M. Enamullah, *Dalton Trans.*, 2009, 3698–3709.

12 M. Enamullah, A. K. M. Royhan Uddin, G. Pescitelli, R. Berardozzi, G. Makhloufi, V. Vasylyeva, A.-C. Chamayou and C. Janiak, *Dalton Trans.*, 2014, **43**, 3313–3329.

13 M. Enamullah, M. A. Quddus, M. R. Hasan, G. Pescitelli, R. Berardozzi, G. J. Reiß and C. Janiak, *Eur. J. Inorg. Chem.*, 2015, 2758–2768.

14 A.-C. Chamayou, S. Lüdeke, V. Brecht, T. B. Freedman, L. A. Nafie and C. Janiak, *Inorg. Chem.*, 2011, **50**, 11363–11374.

15 (*a*) M. Enamullah, V. Vasylyeva and C. Janiak, *Inorg. Chim. Acta*, 2013, **408**, 109–119; (*b*) M. Enamullah and M. K. Islam, *J. Coord. Chem.*, 2013, **66**, 4107–4118.

16 (*a*) M. Enamullah, W. Linert, V. Gutmann and R. F. Jameson, *Monatsh. Chem.*, 1994, **125**, 1301–1309; (*b*) M. Enamullah, W. Linert and V. Gutmann, *Vib. Spectrosc.*, 1995, **9**, 265–271; (*c*) M. Enamullah, F. Renz, U. El-Ayaan, G. Wiesinger and W. Linert, *Vib. Spectrosc.*, 1997, **14**, 95–104; (*d*) M. Enamullah and W. Linert, *J. Coord. Chem.*, 1996, **40**, 193–201.

17 (*a*) M. Enamullah, *J. Coord. Chem.*, 2011, **64**, 1608–1616; (*b*) M. Enamullah, *J. Coord. Chem.*, 2012, **65**, 911–922; (*c*) M. Enamullah, A. K. M. Royhan Uddin and G. Hogart, *J. Coord. Chem.*, 2012, **65**, 4263–4276.

18 M. Enamullah, A.-C. Chamayou and C. Janiak, *Z. Naturforsch.*, 2007, **62b**, 807–817.

19 M. Enamullah, A. K. M. Royhan Uddin, G. Hogarth and C. Janiak, *Inorg. Chim. Acta*, 2012, **387**, 173–180.

20 M. Enamullah, R. Ahmed, G. Makhloufi and C. Janiak unpublished results.

21 S. Yamada, *Coord. Chem. Rev.*, 1999, **190–192**, 537–555.

22 A. Ipatov, F. Cordova, L. J. Doriol and M. E. Casida, *J. Mol. Struct.*, 2009, **914**, 60–73.

23 (*a*) J. Autschbach, in *Comprehensive Chiroptical Spectroscopy*, ed. N. Berova, R. W. Woody, P. Polavarapu and K. Nakanishi, Wiley, New York, 2012, vol. 1, pp. 593–642; (*b*) H. Cox and A. J. Stace, *Int. Rev. Phys. Chem.*, 2010, **29**, 555–588.

24 M. E. Casida, C. Jamorski, K. C. Casida and D. R. Salahub, *J. Chem. Phys.*, 1998, **108**, 4439–4449.

25 C. Janiak, *J. Chem. Soc., Dalton Trans.*, 2000, 3885.

26 (*a*) M. Nishio, *CrystEngComm*, 2004, **6**, 130; (*b*) M. Nishio, M. Hirota and Y. Umezawa, *The CH/π interaction (Evidence, Nature and consequences)*, Wiley-VCH, 1998; (*c*) Y. Umezawa, S. Tsuboyama, K. Honda, J. Uzawa and M. Nishio, *Bull. Chem. Soc. Jpn.*, 1998, **71**, 1207; (*d*) C. Janiak, S. Temizdemir, S. Dechert, W. Deck, F. Girgsdies, J. Heinze, M. J. Kolm, T. G. Scharmann and O. M. Zipffel, *Eur. J. Inorg. Chem.*, 2000, 1229.

27 G. S. Nichol and W. Clegg, *CrystEngComm*, 2007, **9**, 959–960.

28 J. W. Steed, *CrystEngComm*, 2003, **5**, 169–179.

29 A. Gavezotti, *CrystEngComm*, 2008, **10**, 389–398.
30 G. R. Desiraju, *CrystEngComm*, 2007, **9**, 91–92.
31 J. Ruiz, V. Rodríguez, N. Cutillas, A. Hoffmann, A.-C. Chamayou, K. Kazmierczak and C. Janiak, *CrystEngComm*, 2008, **10**, 1928–1938.
32 V. Vasylyeva, T. Kedziorski, N. Metzler-Nolte, C. Schauerte and K. Merz, *Cryst. Growth Des.*, 2010, **10**, 4224–4226.
33 G. Althoff, J. Ruiz, V. Rodríguez, G. López, J. Pérez and C. Janiak, *CrystEngComm*, 2006, **8**, 662–665.
34 X. Hao, S. Parkin and C. P. Brock, *Acta Crystallogr., Sect. B: Struct. Sci.*, 2005, **61**, 689–699.
35 N. J. Babu and A. Nangia, *CrystEngComm*, 2007, **9**, 980–983.
36 A.-C. Chamayou, C. Biswas, A. Ghosh and C. Janiak, *Acta Crystallogr., Sect. C: Cryst. Struct. Commun.*, 2009, **65**, m311–m313.
37 G. Makhloufi, K. Schütte and C. Janiak, *Z. Kristallogr. – New Cryst. Struct.*, 2014, **229**, 429–430.
38 M. T. Kirchner, D. Bläser, R. Boese and G. R. Desiraju, *CrystEngComm*, 2009, **11**, 229–231.
39 S. Roy, R. Banerjee, A. Nangia and G. J. Kruger, *Chem. – Eur. J.*, 2006, **12**, 3777–3788.
40 (*a*) J. O. Hernandez, J. Portilla, J. Cobo and C. Glidewell, *Acta Crystallogr., Sect. C: Cryst. Struct. Commun.*, 2015, **71**, 363–368; (*b*) B. K. Sarojini, H. S. Yathirajan, E. C. Hosten, R. Betz and C. Glidewell, *Acta Crystallogr., Sect. C: Cryst. Struct. Commun.*, 2015, **71**, 59–64.
41 K. M. Anderson, K. Afarinkia, H.-W. Yu, A. E. Goeta and J. W. Steed, *Cryst. Growth Des.*, 2006, **6**, 2109–2113.
42 A.-C. Chamayou, G. Makhloufi, L. A. Nafie, C. Janiak and S. Lüdeke, *Inorg. Chem.*, 2015, **54**, 2193–2203.
43 For examples of metal-chelate ring folding see: B. M. Barry, B. W. Stein, C. A. Larsen, M. N. Wirtz, W. E. Geiber, R. Wateman and R. E. Kemp, *Inorg. Chem.*, 2013, **52**, 9875–9884.
44 M. Enamullah, M. A. Quddus, M. A. Halim, M. K. Islam, V. Vasylyeva and C. Janiak, *Inorg. Chim. Acta*, 2015, **427**, 103–111.
45 (*a*) N. Arai, M. Sorai and S. Seki, *Bull. Chem. Soc. Jpn.*, 1972, **45**, 2398; (*b*) T. Ashida, S. Iwata, T. Yamane, M. Kakudo, A. Takeuchi and S. Yamada, *Bull. Chem. Soc. Jpn.*, 1976, **49**, 3502.
46 M. Enamullah, M. K. Islam, M. A. Halim and C. Janiak, *J. Mol. Struct.*, 2015, **1099**, 154–162.
47 (*a*) S. Dilli, A. M. Maitra and E. Patsalides, *Inorg. Chem.*, 1982, **21**, 2832–2838; (*b*) M. S. El-Shahawi and W. E. Smith, *Analyst*, 1994, **119**, 327–331.
48 (*a*) M. Tumer, D. Ekinci, F. Tumer and A. Bulut, *Spectrochim. Acta, Part A*, 2007, **67**, 916–929; (*b*) N. Mondala, S. Mitra, V. Gramilich, S. O. Ghodsi and K. M. Abdul Malik, *Polyhedron*, 2001, **20**, 135–141.
49 (*a*) H. Sato, A. Yamagishi, J. Yoshida, H. Nakano and N. Hoshino, *Jpn. J. Appl. Phys.*, 2005, **44**, 4067–4072; (*b*) S. Zahn, G. Proni, G. P. Spada and J. W. Canary, *Chem. – Eur. J.*, 2001, **7**, 88–93.
50 APEX2, data collection program for the CCD area-detector system, Version 2.1-0, Bruker Analytical X-ray Systems, Madison (WI), 2006.
51 SAINT, data reduction and frame integration program for the CCD area-detector system, Bruker Analytical X-ray Systems, Madison (WI), 2006.
52 G. Sheldrick, *Acta Crystallogr., Sect. A*, 2008, **64**, 112–122.
53 G. M. Sheldrick, Program SADABS, University of Göttingen, Göttingen, Germany, 1996.
54 K. Brandenburg, Diamond (Version 3.2), Crystal and Molecular Structure Visualization, Crystal Impact, K. Brandenburg & H. Putz Gbr, Bonn, Germany, 2009.
55 (*a*) A. Spek, *Acta Crystallogr., Sect. D: Biol. Crystallogr.*, 2009, **65**, 148–155; (*b*) A. L. Spek, PLATON – A multipurpose crystallographic tool, Utrecht University, Utrecht, The Netherlands, 2005.
56 M. J. Frisch, G. W. Trucks, H. B. Schlegel, G. E. Scuseria, M. A. Robb, J. R. Cheeseman, G. Scalmani, V. Barone, B. Mennucci, G. A. Petersson, H. Nakatsuji, M. Caricato, X. Li, H. P. Hratchian, A. F. Izmaylov, J. Bloino, G. Zheng, J. L. Sonnenberg, M. Hada, M. Ehara, K. Toyota, R. Fukuda, J. Hasegawa, M. Ishida, T. Nakajima, Y. Honda, O. Kitao, H. Nakai, T. Vreven, J. A. Montgomery, J. E. Peralta, F. Ogliaro, M. Bearpark, J. J. Heyd, E. Brothers, K. N. Kudin, V. N. Staroverov, R. Kobayashi, J. Normand, K. Raghavachari, A. Rendell, J. C. Burant, S. S. Iyengar, J. Tomasi, M. Cossi, N. Rega, J. M. Millam, M. Klene, J. E. Knox, J. B. Cross, V. Bakken, C. Adamo, J. Jaramillo, R. Gomperts, R. E. Stratmann, O. Yazyev, A. J. Austin, R. Cammi, C. Pomelli, J. W. Ochterski, R. L. Martin, K. Morokuma, V. G. Zakrzewski, G. A. Voth, P. Salvador, J. J. Dannenberg, S. Dapprich, A. D. Daniels, Ö. Farkas, J. B. Foresman, J. V. Ortiz, J. Cioslowski and D. J. Fox, *Gaussian 09, Revision C.01*, Wallingford CT, 2009.
57 All references about DFT functionals and basis sets can be found in the on-line documentation for Gaussian'09 at http://www.gaussian.com/g_tech/g_ur/g09help.htm.
58 T. Bruhn, A. Schaumlöffel, Y. Hemberger and G. Bringmann, *Chirality*, 2013, **25**, 243–249.
59 (*a*) H. D. Flack, M. Sadki, A. L. Thompson and D. J. Watkin, *Acta Crystallogr., Sect. A*, 2011, **67**, 21–34; (*b*) H. D. Flack and G. Bernardinelli, *Chirality*, 2008, **20**, 681–690; (*c*) H. D. Flack and G. Bernardinelli, *Acta Crystallogr., Sect. A*, 1999, **55**, 908–915; (*d*) H. D. Flack, *Acta Crystallogr., Sect. A*, 1983, **39**, 876–881.

